Device

Article

The Electrolab: An open-source, modular platform for automated characterization of redox-active electrolytes

Graphical abstract

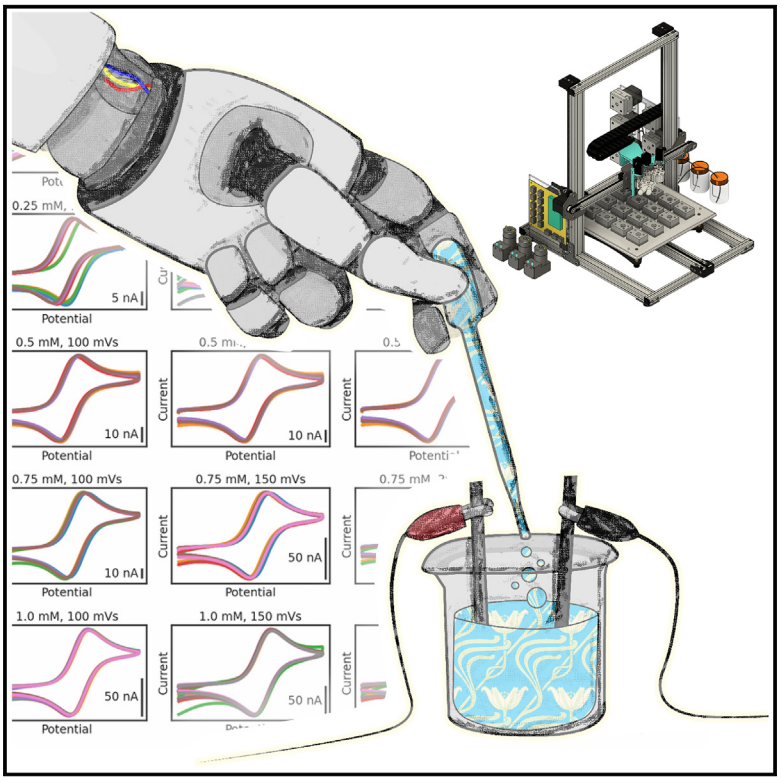

Highlights

- DIY solution-handling robot, electrochemical multiplexer, and Python libraries
- Benchmark of 200 voltammograms across a range of conditions in 2 h
- Experiment featuring sub-nA, non-aqueous, redox electrolyte measurements

Authors

Inkyu Oh, Michael A. Pence, Nikita G. Lukhanin, Oliver Rodríguez, Charles M. Schroeder, Joaquín Rodríguez-López

Correspondence

cms@illinois.edu (C.M.S.), joaquinr@illinois.edu (J.R.-L.)

In brief

The Electrolab is introduced as a versatile, automated, electroanalytical platform using a solution-handling robot, Python software, and microfabricated electrodes to accelerate the characterization and discovery of molecules for energy storage and conversion. Its modularity will enable its use for laboratory automation beyond electrochemical characterization, and its open-source nature will encourage shareable routines and coupling to data analysis and discovery algorithms.

Develop
Prototype with demonstrated applications in relevant environment

Oh et al., 2023, Device *1*, 100103
November 17, 2023
https://doi.org/10.1016/j.device.2023.100103

CellPress

Please cite this article in press as: Oh et al., The Electrolab: An open-source, modular platform for automated characterization of redox-active electrolytes, Device (2023), https://doi.org/10.1016/j.device.2023.100103

Device

CellPress
OPEN ACCESS

Article

The Electrolab: An open-source, modular platform for automated characterization of redox-active electrolytes

Inkyu Oh,[1,5,6] Michael A. Pence,[1,2,5,6] Nikita G. Lukhanin,[1,2,5,6] Oliver Rodríguez,[1,2,5,6] Charles M. Schroeder,[1,2,3,4,5,*] and Joaquín Rodríguez-López[1,2,5,7,*]

[1]Beckman Institute for Advanced Science and Technology, University of Illinois at Urbana-Champaign, Urbana, IL 61801, USA
[2]Department of Chemistry, University of Illinois at Urbana-Champaign, Urbana, IL 61801, USA
[3]Department of Chemical and Biomolecular Engineering, University of Illinois at Urbana-Champaign, Urbana, IL 61801, USA
[4]Department of Materials Science and Engineering, University of Illinois at Urbana-Champaign, Urbana, IL 61801, USA
[5]Joint Center for Energy Storage Research (JCESR), Argonne, IL 60439, USA
[6]These authors contributed equally
[7]Lead contact
*Correspondence: cms@illinois.edu (C.M.S.), joaquinr@illinois.edu (J.R.-L.)
https://doi.org/10.1016/j.device.2023.100103

THE BIGGER PICTURE Pressing environmental challenges and the rising integration of renewable electricity into chemical technology have rendered electrochemistry ubiquitous, making new tools for the accelerated exploration and discovery of redox-active molecules and materials essential. Ideally, these tools should benefit from advances in other areas, such as artificial intelligence, and could be designed with an open-source mindset that encourages easy sharing and reproduction of experimental explorations. We designed the Electrolab with these characteristics in mind. Here, we present it as an automated platform that integrates a solution-handling robot, Python software, and microfabricated electrodes to characterize redox-active electrolytes in a versatile manner and with minimal supervision. Of interest to the broader device community, we provide instructions to convert a 3D printer into a solution-handling robot, making the Electrolab highly affordable for applications in energy storage and conversion.

SUMMARY

Electrochemical characterization of redox-active molecules in solution requires exploration of manifold conditions (e.g., concentration, electrolyte type, pH, ionic strength), leading to tedious and time-consuming experiments that are prone to user error. Here, we introduce the Electrolab, a modular, automated electrochemical characterization platform that seamlessly interfaces with common laboratory instrumentation and low-cost electromechanical components. We integrated a gantry-type robot carrying a multipurpose nozzle assembly to dispense and mix solutions as well as degas and clean a cell containing multiplexed microelectrochemical arrays. The system operates using Python code and a universal Arduino-based controller. We demonstrate the Electrolab by autonomously analyzing a redox mediator by performing 200 voltammograms and data analysis steps across a range of conditions. In addition, the Electrolab is used to titrate a redox-active polymer solution to identify conditions for optimizing electrochemical performance. Overall, the Electrolab device enables high-throughput, systematic exploration of redox electrolytes, opening new avenues for closed-loop optimization.

INTRODUCTION

Automated experimental systems hold strong promise to reduce the human effort required for the discovery of next-generation materials for energy conversion and storage.[1] The use of artificial intelligence, combined with automated synthesis and characterization, has recently enabled accelerated studies of materials, including conjugated oligomers, photovoltaic thin films, and metallic nanoparticles.[2–4] Given the growing demand for energy storage applications, automated characterization methods for electrochemical studies would greatly accelerate efforts toward autonomous discovery of new materials.

Redox-flow battery (RFB) materials, in which molecules are dissolved in a variety of aqueous or non-aqueous electrolytes,[5–7]

Please cite this article in press as: Oh et al., The Electrolab: An open-source, modular platform for automated characterization of redox-active electrolytes, Device (2023), https://doi.org/10.1016/j.device.2023.100103

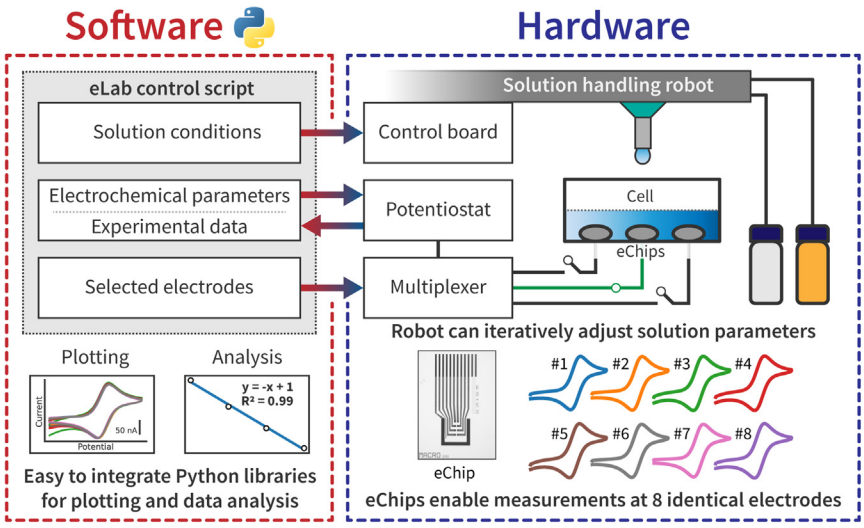

Figure 1. Schematic depicting an overview of Electrolab operation and the relationship between the software and hardware components

A control script controls the experimental workflow and parameters. The Electrolab API translates code to commands readable by the Electrolab hardware. The hardware performs the desired solution/gas operations while electrochemical measurements are performed. The use of multiplexed microfabricated arrays (eChips) enables replicate measurements.

are prime candidates for study by automated platforms. The chemical space of potential materials for use in RFBs is vast, consisting of materials such as posolytes and negolytes (electrolytes used to store charge at the positive and negative terminals of the battery, respectively), small-molecule monomers, oligomers, and redox-active polymers and colloidal particles.[7–15] The solution conditions (e.g., solvent and electrolyte type, pH, ionic strength, and the presence of dissolved gases) dramatically affect battery performance, notably the electron transfer kinetics, stability, and transport.[16–19] The dependence of battery performance on solution conditions requires multiobjective optimization of parameters, including the concentration of electroactive materials, the ionic strength and composition of supporting electrolyte, and the choice of solvent.[18] To address these challenges, automated platforms for electrochemical characterization can be used to enable rapid exploration of the expansive chemical space, allowing candidate RFB materials to be efficiently identified. In recent years, a variety of automated and high-throughput platforms for characterizing battery materials have been developed.[20–24] For example, studies of fast-charging lithium-ion battery electrolytes were performed using a robotic platform relying on Bayesian optimization to guide experiments.[22] In addition, an automated experimental platform was also used to optimize supporting electrolyte and solvent composition for conductivity and solubility of redox-active species, but electrochemical characterization was only performed using the optimized solution conditions.[23]

Prior work has also used robotics to automate electrochemical characterization experiments. In one case, an XYZ gantry robot was used to move a bundle of three electrodes between the wells of a microtiter plate.[25–28] In addition, new electrochemical instrumentation was recently developed to simultaneously perform voltammetry measurements on 96 electrochemical cells, thereby providing a highly parallel and non-mechanical analogue to XYZ gantry robots.[29] These platforms enable efficient screening of a moderate chemical space, but the predefined electrode geometries and solution conditions limit the scope of possible experiments and generally do not allow closed-loop discovery approaches, where experimental results from a prior round are used to automatically determine the parameters in the next round of an iterative campaign.

Here, we report an automated electrochemical characterization platform called the Electrolab, consisting of fluidic, electrochemical, and software modules as individual subsystems (Figure 1). A distinguishing feature of our platform is the incorporation of microfabricated electrodes into the experimental workflow. Microelectrode geometries have characteristics that greatly benefit electrochemical analysis, such as decreased charging current, the ability to probe processes at sub-millisecond timescales, and the ability to make electrochemical measurements in resistive solutions.[30] The hardware components of the platform include a solution-handling robot, microfabricated electrode arrays (eChips), an electrode multiplexer, and a potentiostat. The software module consists of a custom application programming interface (API) developed in Python that interfaces to the Electrolab hardware and enables users to program experimental routines using a Python script.[31] The software module expands beyond hardware control by interfacing with third-party Python libraries, offering fully automated data analysis, plotting, and the potential for integration with machine learning (ML) algorithms. The use of Python scripts to control experiments and analysis allows transfer of the experimental workflow between researchers, providing a means to assess reproducibility across laboratories and a record of performed experiments and experimental parameters. The Electrolab was designed with modularity and accessibility in mind, incorporating open-source software and readily available, adaptable, and affordable hardware. The ability to use high-level commands to universally control different hardware components furthers our goal of transferability, allowing near-identical experiments to be performed across different instrumental setups. All modules of the Electrolab can be used independently from each other and can be easily integrated with common electrochemical instruments in research laboratories.

RESULTS AND DISCUSSION

Hardware design

The Electrolab platform is highly modular and compatible with electrochemical and mechanical hardware that can be controlled

Please cite this article in press as: Oh et al., The Electrolab: An open-source, modular platform for automated characterization of redox-active electrolytes, Device (2023), https://doi.org/10.1016/j.device.2023.100103

(directly or indirectly) by Python scripts. The custom solution-handling robot and its components are shown in Figure 2A. The robot is constructed almost entirely from generic components, aside from the XYZ gantry frame, which was taken from a commercial 3D printer. We developed a universal control board for the generic electromechanical components, shown in Figure 2B. The board is controlled by an Arduino Mega microcontroller with inputs for sensors and limit switches and output drivers for the solenoids and motors used in the solution-handling robot, as shown in Figure S1. This control board provides a link that enables the Python API to control readily available mechanical components without needing specialized driver boards for each pump, motor, or valve. This level of integration increased flexibility and reduced costs because the platform was built by assembling generic components (Table S2) instead of requiring interfacing with expensive commercial robotic solution-handling platforms. Our approach also increases transferability between labs because high-level control scripts can be shared regardless of the precise hardware used for robotics.

The electrochemistry module is built around microfabricated, individually addressable electrode arrays, to which we refer as eChips. The eChips are placed into electrochemical cells and can be individually addressed using a reed-relay based multiplexer, as shown in Figure 2C. The multiplexer is compatible with most commercial potentiostats and is controlled by an onboard Arduino Uno through serial communication. The KiCad files and parts list (Table S3) for the multiplexer, as well as STL files for the electrochemical cells, are available in the supplemental information.

The use of microfabricated electrode arrays allows incorporation of multiple pristine electrodes in one electrochemical cell. Some redox flow battery electrolytes have been shown to adsorb onto electrode surfaces,[32] and fouling of the electrode surface is a major concern that may lead to distorted electrochemical signals. For these reasons, pristine electrode surfaces are required for electrochemical analysis. The use of individually addressable electrode arrays circumvents the need for an additional cleaning step, assuming that there are enough electrodes available for the desired number of experiments. If electrode fouling is not an issue, then the use of multiple electrodes allows replicate data to be easily obtained, enabling the user to perform statistical analysis. In addition, microfabrication allows us to tailor electrode design to enable specific experimental routines, such as using interdigitated arrays to perform characterization of redoxmer stability under different solution conditions.[33] However, the use of microfabricated and multiplexed electrodes is not a requisite for the platform because the electrochemical cells can be designed to accommodate other electrode types. Because of the modular nature of our platform, we modified the electrochemical cell designs to accommodate both ultramicroelectrodes and screen-printed electrodes, as described below.

A unique aspect of our robot is the nozzle assembly, which adds a high degree of versatility to the platform. The XYZ gantry moves a set of nozzle heads to the chosen electrochemical cell and then performs fluidic operations on the desired cell. The robot was designed to accommodate four nozzles; however, only three are used for dispensing, rinsing, and gas (argon) operations. Figure 2D shows a labeled photo of the fluidic nozzles. The remaining nozzle head can be modified with additional fluidic lines or probes for a variety of purposes, including connection to external instruments, measuring pH, or inserting a reference electrode with a salt bridge.

The dispensing nozzle can dispense up to three separate solution lines, driven by peristaltic pumps. Solutions were contained in glass medium bottles with two-port caps and delivered through polytetrafluoroethylene (PTFE) tubing to 23G, 0.5-in stainless steel dispensing needles. The peristaltic pumps were calibrated gravimetrically for accurate volume dispensing and showed from −0.2% to +3.5% error for the averaged dispensed mass (n = 3) of five different volumes of water (100 μL, 150 μL, 300 μL, 500 μL, and 1 mL; Figures S4 and S5; Tables S4 and S5). An empirical correction factor was used for peristaltic pump operation because of an apparent nonlinearity between the target and actual dispensed volumes (Figure S7). Additional details regarding dispensing accuracy are described in Notes S4 and S5. Each dispensing line is individually connected to the corresponding solution sample reservoir to avoid sample cross-contamination.

The rinsing nozzle was designed to remove solution after testing while simultaneously flushing the electrochemical cell with clean solvent. The rinsing nozzle contains two separate internal fluidic channels for suction and flushing, enabling constant flow of solvent for cleaning purposes. Volumetric flow rates for suction and flushing were measured by tracking water displacement in a graduated container and were found to be 0.46 mL/s and 0.11 mL/s, respectively. Clean solvent was delivered to the rinsing nozzle by a peristaltic pump, and used solvent was evacuated by pressure-driven flow using a DC pneumatic pump to pull a vacuum inside of the waste bottle.

The argon nozzle has two operating modes: sparging mode and drying mode. The sparging mode bubbles a 0.26-sccm flow rate of argon into the cell, which simultaneously displaces oxygen and mixes the dispensed solutions. The drying mode uses a 3.0-sccm flow of argon to help dry any solution that remains in the electrochemical cell after the cleaning procedure. Two normally closed solenoid valves were used to control argon flow. A representative video illustrating how the three nozzles are used during an automated experiment is shown in Video S1, and a sequential flowchart with snapshots from this video is shown in Figure 3A.

We performed an automated control experiment as depicted in Figure 3B to demonstrate the efficacy of the rinsing routine of our experimental workflow. We first performed cyclic voltammetry (CV) with 100 mM KNO_3-supporting electrolyte solution. Next, CVs were performed using a solution of 1 mM redox species hydroxymethylferrocene (FcMeOH) along with 100 mM KNO_3. Finally, CV was performed on the same 100 mM KNO_3 solution following rinsing. The CVs in Figure 3B are the average (n = 8) of eight identical 200-μm Pt electrodes, sweeping from −0.2 to 0.3 to −0.2 V at a scan rate of 100 mV/s. The CVs of supporting electrolyte before and after FcMeOH dispensing are almost identical and show no visible indications of sample carryover between runs.

Following demonstration of device operation and validation, we next focused on two experiments establishing the capabilities and versatility of our platform: systematic exploration of

Please cite this article in press as: Oh et al., The Electrolab: An open-source, modular platform for automated characterization of redox-active electrolytes, Device (2023), https://doi.org/10.1016/j.device.2023.100103

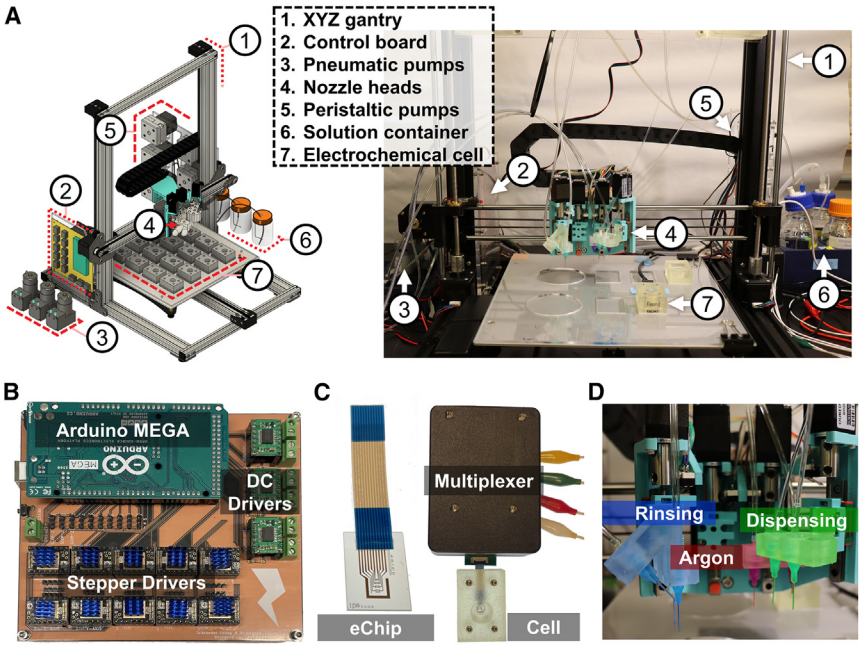

Figure 2. Hardware modules of the Electrolab

(A) 3D model of the Electrolab solution-handling robot and the fully assembled robot with labeled components.

(B) Universal electromechanical control board with an Arduino Mega microcontroller, DC drivers, and stepper motor drivers.

(C) Components of the electrochemical module: microfabricated eChip electrode arrays, the electrochemical cell, and the multiplexer that selects between the different electrodes.

(D) Fluidic nozzle system mounted on the XYZ gantry, with all nozzles able to be moved up/down individually. Nozzles are responsible for dispensing and disposing of fluids, rinsing and flushing with solvent, and drying or sparging with argon.

redox-active transport through verification of the Randles-Ševčík equation and optimization of the current observed in a redox-active polymer solution as a function of ionic strength.

Automated determination of transport and reaction parameters for a redox species

We first used the Randles-Ševčík formalism to experimentally benchmark the performance of the Electrolab using a well-known redox species (FcMeOH). This benchmark experiment allows us to demonstrate the capabilities of the Electrolab to obtain and analyze a large set of results to uncover statistical distributions within a nominally simple experiment. FcMeOH shows electrochemically and chemically reversible behavior when typical voltametric scan rates ($v \ll 10$ V/s) are employed and has a previously reported diffusion coefficient of 7.6×10^{-6} $cm^2/s \pm 0.3 \times 10^{-6}$ cm^2/s (n = 5, 25°C).[34–38] We set up the robot to dispense two different aqueous solutions: one solution containing 1 mM FcMeOH and 100 mM KNO_3-supporting electrolyte and the other solution containing solely 100 mM KNO_3. We used an electrode array consisting of eight 200-μm diameter electrodes to perform CV at different concentrations and scan rates. The robot prepared one of five concentrations of FcMeOH (0, 0.25, 0.5, 0.75, or 1.0 mM) and then selected one of the 8 electrodes on the chip and ran CVs at five scan rates (50, 100, 150, 200, and 250 mV/s), sweeping from −0.2 to 0.3 to −0.2 V. The loop automatically iterated through all 200 combinations of concentrations, electrodes, and scan rates.

A total of 200 CVs, along with cleaning and drying of the electrochemical cell before the next concentration was prepared, were performed over approximately 2 h. During the process of data acquisition, CVs were automatically analyzed at each scan rate and concentration for all eight electrodes, enabling determination of the mean and standard deviation for four key features, including the minimum and maximum peak currents, peak positions, and peak separation. Key features that had values more than 2 σ from the mean were identified as outliers (30 CVs were identified as outliers). CVs with outliers removed are shown in Figure 4A (raw data and experimental scripts are available in the supplemental information). Figure S8 shows the complete dataset with no outliers removed. The mean peak currents of the nonoutlier CVs were plotted as a function of the square root of scan rate for all concentrations, and a linear regression was performed, as shown in Figure 4B. The expected results should conform to the linear diffusion model described by the Randles-Ševčík equation at 25°C,

$$i_{peak} = 2.69 \times 10^5 n^{3/2} AC\sqrt{Dv}$$

where n is number of electrons transferred, A is electrode area in cm^2, C is concentration in mol/cm^2, D is diffusion coefficient in cm^2/s, and v is the scan rate in V/s.

Linear regressions generally showed large R^2 values (>0.995) and relatively small intercepts (<2.5% of the slope) for all concentrations of FcMeOH present in solution, which indicates that the electrochemical reaction is diffusion controlled. The values of the intercept, the intercept relative to the slope, and the R^2 of the regressions are shown in Table S6. Plots of peak current as a function of FcMeOH concentration are shown in Figure S9 and were also highly linear (Table S7). The average peak separation, ΔE, was determined as 67 mV with a standard deviation of 37 mV, which is slightly larger than the expected 59 mV peak separation for an electrochemically reversible one-electron system.[39] The diffusion-controlled behavior and the apparent electrochemical reversibility indicate that use of the Randles-Ševčík equation to determine the diffusion coefficient of the redox species is justified.

Figure 4C shows a histogram with diffusion coefficients of all non-outlier CVs calculated using the Randles-Ševčík equation (Equation 1). The mean diffusion coefficient was determined to be 7.1×10^{-6} cm^2/s with a standard deviation of 0.6×10^{-6} cm^2/s. This value is in line with reported diffusion coefficient

Please cite this article in press as: Oh et al., The Electrolab: An open-source, modular platform for automated characterization of redox-active electrolytes, Device (2023), https://doi.org/10.1016/j.device.2023.100103

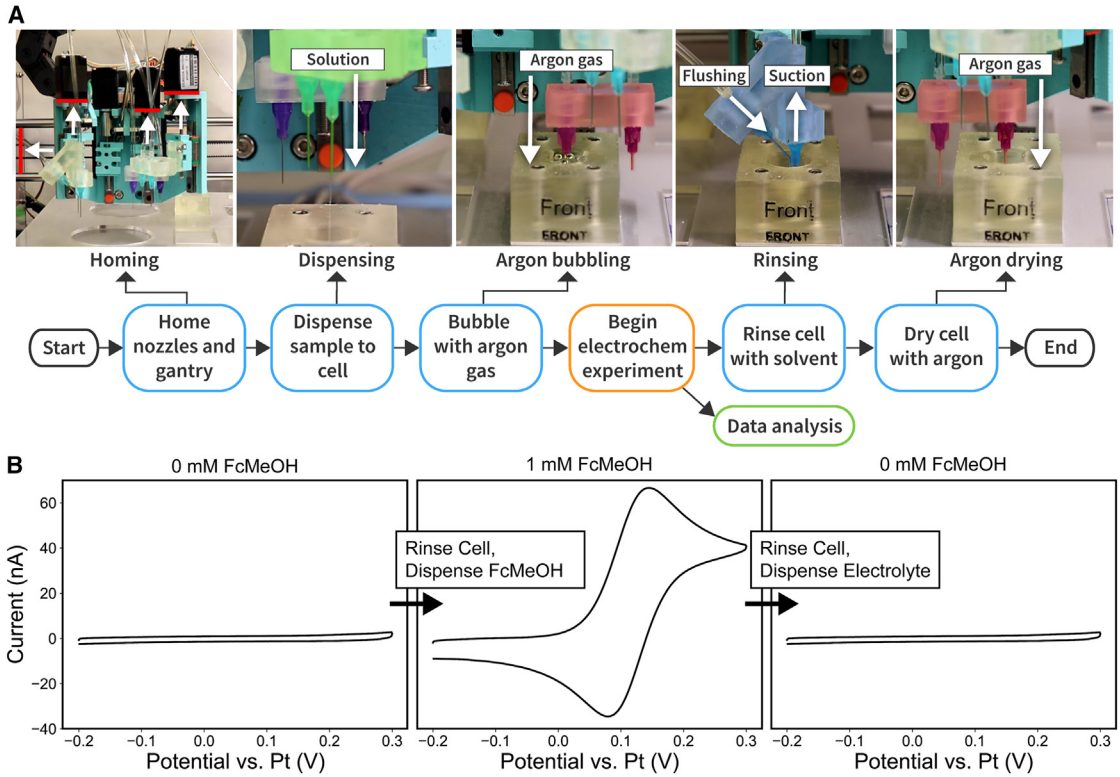

Figure 3. Overview of the Electrolab workflow

(A) A flowchart describing a typical routine for an automated electrochemical experiment. Pictures show snapshots of the robot performing homing, dispensing, bubbling, rinsing, and drying operations.

(B) A control experiment with cyclic voltammetry (CV) to assess potential cross-contamination upon successive measurements on the same electrochemical cell. Shown first are the averaged CVs (n = 8) of 100 mM KNO_3 supporting electrolyte (left), the response upon replacement of solution with 1 mM hydroxymethylferrocene (FcMeOH) and 100 mM KNO_3 (center), and a repeated experiment with 100 mM KNO_3 supporting electrolyte (right) after the cell was subjected to the rinsing routine. Voltammograms were recorded at a scan rate of 100 mV/s using an electrode array (eChip) with eight identical 200-μm-diameter Pt working electrodes.

values of 7.6 × 10^{-6} cm^2/s for FcMeOH.[34–38] The Electrolab automated exploration enables the user to decide on the most appropriate statistical reasoning to analyze the data. For example, the diffusion coefficient can be determined based on individual peak current values, but one could also perform regression analysis of the slope of the current versus concentration or slope of the current versus scan rate (Tables S6 and S7) in the Randles-Ševčík formalism. These methods yield similar but slightly different values for the diffusion coefficient because they consider the effects of experimental errors differently. Nevertheless, a one-way ANOVA test finds no significant difference between the diffusion coefficients determined using these different methods. Figures S10 and S11 show boxplots of the calculated diffusion coefficients as a function of concentration and scan rate, respectively. From Figure S10, the diffusion coefficient values for the 0.5 mM and 0.75 mM FcMeOH solutions are notably smaller than those of 0.25 mM and 1 mM FcMeOH solutions, indicating that the variation in solution concentration impacted the measured diffusion coefficient and contributed to measuring error. The variation in concentration likely arises from error in dispensed solution volumes (Figure S6), but these issues can be identified because of the large sets of data conveniently generated by the Electrolab, thus providing the opportunity to apply corrective measures as needed. Dispensing accuracy can be improved by using higher-performance pumps, such as a piston-driven syringe pump, but this will increase the overall cost of the fluidic components.

Figure S11 shows a smaller difference between the diffusion coefficient values for the different scan rates, apart from notably larger values at 50 mV/s. Boxplots of peak-to-peak separation, ΔE, are also plotted as a function of scan rate in Figure S12, and lower scan rates show increased values of ΔE. This behavior is due to deviation from transient voltametric conditions at the relatively small 200-μm electrodes, leading to distortion of the voltammograms at slower scan rates.[40] Nevertheless, the relatively small geometric dimensions of the electrodes provide benefits in the form of reduced charging currents and reduced voltage drop due to solution resistance compared with typical commercial macroelectrodes, which often have diameters of a few millimeters. However, the Electrolab's versatility is further enhanced by its capacity to incorporate commercial macroelectrodes by adapting the electrochemical cell's geometry. Figures S14 and S15 show the results of an automated electrochemical experiment with a screen-printed

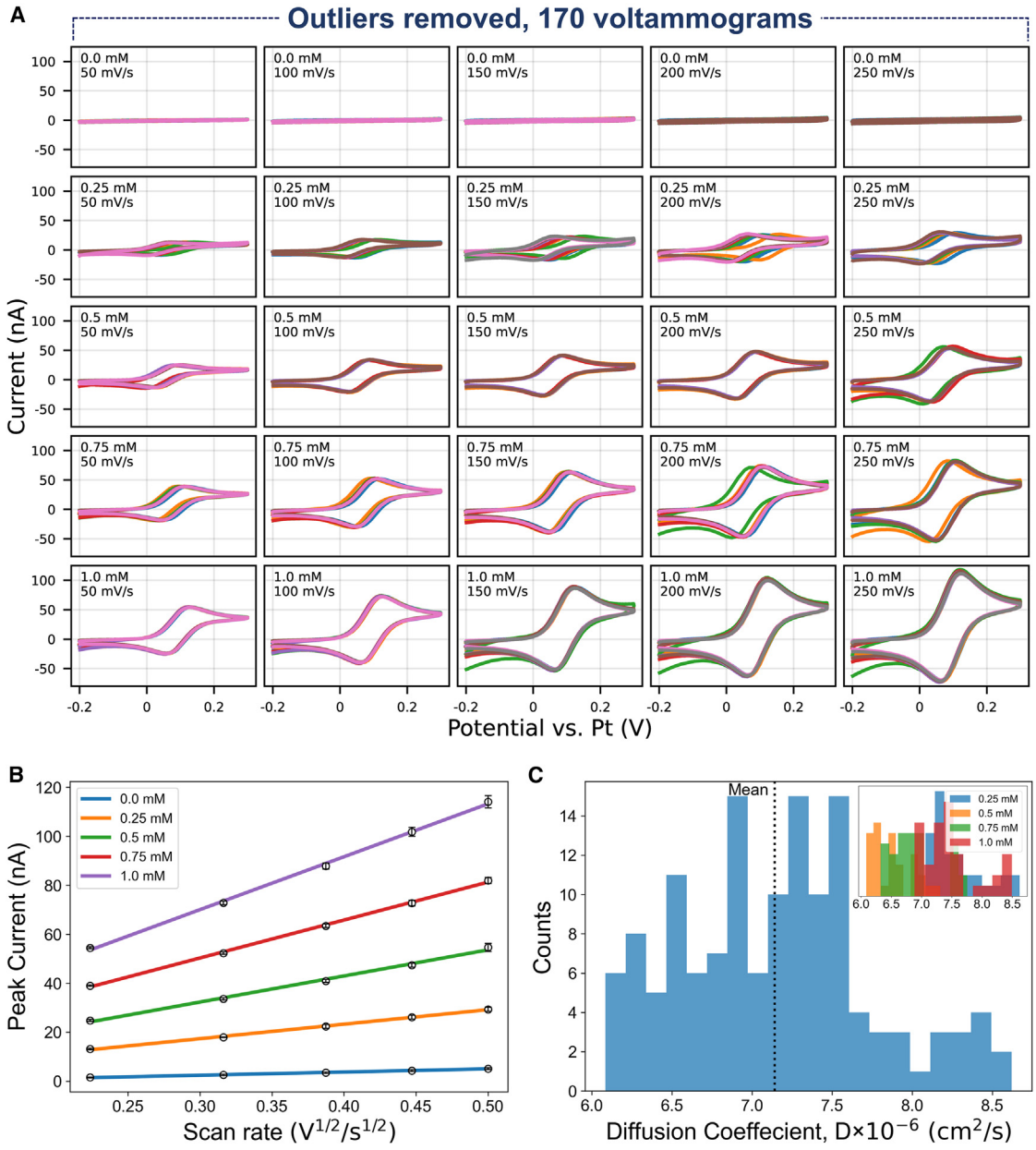

Figure 4. Results of automated experiments with FcMeOH

(A) CV at five different scan rates (50, 100, 150, 200, and 250 mV/s) and five different concentrations (0, 0.25, 0.5, 0.75, and 1.0 mM) with eight identical electrodes on one eChip. Shown are 170 voltammograms after the 30 outlier voltammograms were identified and removed.

(B) Average peak currents (outliers removed) plotted as a function of the square root of the scan rate at five different redox species concentrations. The error bars represent one standard deviation from the mean.

(C) Histogram of diffusion coefficients calculated using the Randles-Ševčík equation, with a mean value of 7.1 × 10^{-6} cm^2/s. The inset shows overlaid histograms of calculated diffusion coefficients for the different dispensed solution concentrations.

electrode, which are further described in Note S6. Screen-printed electrodes are generally inexpensive; however, batch-to-batch variability leads to potential issues in quantitative electrochemical characterization.

From Figure 4A, the $E_{1/2}$ values of the voltammograms at lower concentrations show more variation compared with higher concentrations. Figure S13 shows boxplots of $E_{1/2}$ values at different concentrations. This variation in $E_{1/2}$ arises because of the use of a Pt wire quasi-reference electrode, which is not as stable as a true reference electrode. This issue can be solved by mounting a true reference electrode and salt bridge onto one of the nozzles and lowering it into solution while electrochemical experiments are performed. Incorporation of a real reference electrode is planned for future versions of the platform.

Please cite this article in press as: Oh et al., The Electrolab: An open-source, modular platform for automated characterization of redox-active electrolytes, Device (2023), https://doi.org/10.1016/j.device.2023.100103

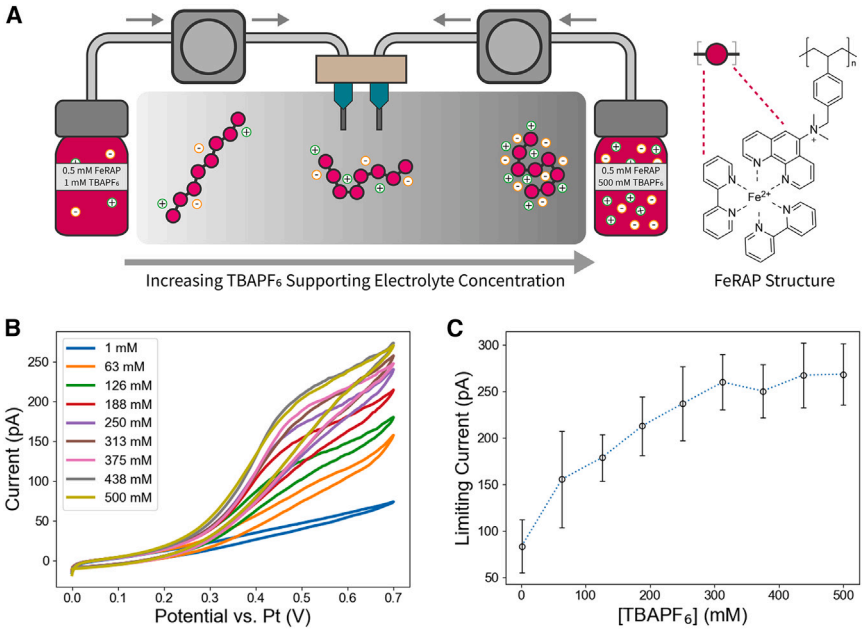

Figure 5. Automated characterization experiments with Fe-RAP in varying concentrations of $TBAPF_6$ supporting electrolyte obtained with a 25-μm-diameter Au UME

(A) Schematic depicting the experimental workflow, where the Electrolab dispenses an Fe-RAP solution with a constant 0.5 mM concentration of Fe-RAP but a desired supporting electrolyte concentration.

(B) Average cyclic voltammograms (n = 5) for different concentrations of $TBAPF_6$, obtained at a scan rate of 5 mV/s.

(C) Average steady-state currents (n = 5) obtained from a 60-s chronoamperometric curve plotted against the concentration of $TBAPF_6$. Error bars represent one standard deviation.

Titration of supporting electrolyte for optimal redox-active polymer performance

The Electrolab enables the study and optimization of the performance of redox flow battery materials by automated tuning of solution conditions. Here we used the Electrolab to understand the effect of supporting electrolyte concentration on the current generated by the electrolysis of redox-active polymers at an electrode surface. We have established that the supporting electrolyte concentration changes the conformational structure of charged redox-active polymers, which, in turn, affects charge transfer dynamics along the polymer chain and the current measured at the electrode.[41,42] Here, we focus on an iron-based redox-active polymer (Fe-RAP) candidate for a nonaqueous RFB and used the Electrolab to perform a grid search across a finite range of concentrations of supporting electrolyte to identify the concentration that leads to the highest current. Grid search experiments of this type are tedious to perform manually but are easily managed using automated solution handling.

The solution-handling robot was interfaced with two solutions of 0.5 mM Fe-RAP in acetonitrile (to maintain the redox-active component at constant concentration) but with one solution containing 1 mM $TBAPF_6$ and the other solution containing 500 mM $TBAPF_6$ to vary the ionic strength, as depicted in Figure 5A. The solutions were dispensed and mixed to obtain 9 different concentrations ranging from 1–500 mM, in 62.4-mM increments. The experiment was repeated 5 times to obtain replicate data, polishing the ultramicroelectrode before each run. The order of dispensed concentrations was randomly shuffled before each automated experiment to reduce the potential impact of undesirable side processes that could have sequential effects (e.g., electrode fouling). CVs and chronoamperometry were performed at each concentration of supporting electrolyte. CVs were swept from 0 to 0.7 to 0 V at a scan rate of 5 mV/s to ensure steady-state behavior and minimize contributions from transient surface processes. Chronoamperometry was performed by applying a potential of 0.7 V for 60 s, and the limiting current was sampled after 60 s. Because of the versatility and modularity of our platform, we fabricated an electrochemical cell that incorporated a 25-μm Au ultramicroelectrode (UME) working electrode and a Pt wire counter-reference electrode.

Figure 5B shows the average (n = 5) CVs obtained at each supporting electrolyte concentration (raw data and the experimental script are available in the supplemental information). All CVs show sigmoidal behavior that is characteristic of UME voltammetry. Figure 5C shows the steady-state current obtained by chronoamperometry as a function of supporting electrolyte concentration. Our results show that the steady-state current increases with the supporting electrolyte concentration until leveling off above 400 mM of $TBAPF_6$. In general, this electrochemical behavior is not easily described by an analytical expression and is challenging to predict, which necessitates manual exploration to determine the optimal concentration of supporting electrolyte. Remarkably, all experiments shown in Figure 5 only required 3.5 h to evaluate 9 supporting electrolyte concentrations using a fully automated approach. However, these experiments were performed with strict rinsing procedures between electrochemical measurements, and this particular experiment used a relatively low scan rate, which would make the entire campaign extremely tedious to perform using manual experimentation. In addition, the experiment did not require intervention or action by human researchers; as a consequence, the researchers were able to monitor the experiments remotely (from outside of the lab), which is advantageous because of the low measured currents, which makes the experiment susceptible to electrical and mechanical noise (additional noise mitigation details are described in Note S7 and Figure S16). From this view, the Electrolab allows low-supervision experimental capabilities for automated electrochemical characterization. In addition, we note that this platform handles non-aqueous conditions at relatively high concentration of supporting electrolyte (0.5 M), a critical requirement for studying non-aqueous redox flow battery materials.

Please cite this article in press as: Oh et al., The Electrolab: An open-source, modular platform for automated characterization of redox-active electrolytes, Device (2023), https://doi.org/10.1016/j.device.2023.100103

Conclusions

In this work, we report the development and demonstration of an automated electrochemical platform for characterization of redox-active species in solution. The Electrolab is constructed from widely available and inexpensive components and uses open-source software, making it highly accessible to interested researchers. By using microfabricated electrode arrays, it is possible to have several pristine electrodes in a single electrochemical cell, which can be interchanged throughout the experiment, facilitating data replication and statistical analysis. We further demonstrate the use of other electrode types, such as UMEs and screen-printed macroelectrodes. Coordination of accurate dispensing with electrochemistry enables closed-loop experimentation, which is challenging, if not impossible, for well-plate-type robots[25–28] because the desired solution composition is preset in such systems and cannot be changed on the fly. In addition, the nozzle system allows versatile operations beyond simple fluid dispensing, such as sparging solutions with argon gas and cleaning of cells with solvent. The nozzle system also offers additional flexibility by accommodating various probe-like attachments such as thermocouples, pH meters, and reference electrodes in salt bridges. Future work will incorporate probe-like attachments with the nozzle system to expand the analytical capabilities of the platform. For these reasons, the Electrolab offers multiple key features that will be useful for other researchers to use for automated electrochemistry systems.

As a proof-of-principle demonstration, we used FcMeOH as a benchmark redox species for electrochemical characterization. Using the Electrolab, we experimentally determined a value for the diffusion coefficient that is in good agreement with previously reported values. We performed 200 voltammograms in a single experiment, including the automated acquisition of experimental data, plotting, and analysis over the span of 2 h, which would otherwise be a daunting task for an experimenter using manual experimentation. We further used the Electrolab for an electrolyte titration experiment, identifying optimal solution conditions for redox polymer performance. To expand the capabilities of our platform beyond what we have demonstrated in this work, we plan to modify the solution-handling robot with fluidic selector valves and a more compact frame that can fit inside a glovebox. This will further enhance the ability of our platform to study redox flow battery materials by enabling studies of larger sample libraries in an inert and air-free environment.

In future work, we aim to incorporate data science methods with the Electrolab for fully autonomous electrochemical characterization. Electrochemistry has seen an emergence of ML-based methods in recent years, particularly in the development of deep-learning algorithms that will aid in characterizing electrochemical reaction mechanisms.[43–45] Additionally, algorithms such as Bayesian optimization, which have been successfully employed in fields such as automated synthesis, will allow optimization of solution conditions with much higher efficiency compared with random sampling or exhaustive grid searches.[46,47] The availability of Python libraries for ML will make incorporation into the Electrolab workflow simple. The Electrolab holds strong promise to enable digitization of electrochemical workflows, allowing procedures to be shared among experimenters despite potential differences in electrochemical and solution-handling hardware. The ability to share scripts among researchers will provide transparency, and means to easily reproduce experiments are critically needed in scientific research.[48–50] Automated electrochemistry is a relatively underexplored area, and we believe that the versatile and relatively inexpensive nature of the Electrolab will provide many researchers with a starting point to incorporate automated electrochemistry into a diverse array of experimental systems.

EXPERIMENTAL PROCEDURES

Resource availability

Lead contact

Further information and requests for resources should be directed to and will be fulfilled by the lead contact, Joaquín Rodríguez-López (joaquinr@illinois.edu).

Materials availability

This study did not generate new materials.

Data and code availability

All raw electrochemical data reported in this paper are available on Mendeley Data: https://doi.org/10.17632/cvm9y582tf.1,[51] in the supplemental information, and/or will be shared by the lead contact upon request. All original code is available in this paper's supplemental information and/or can be found on Zenodo: https://www.doi.org/10.5281/zenodo.8323222.[52]

Chemicals and materials

Deionized water (18 MΩ resistance) was obtained from a Milli-Q purification system. The Fe-RAP was synthesized as described in Note S1 and used as provided. All other chemicals were purchased commercially and used as received. SPR 220, LOR5A, KMPR 1010 photoresists, SU8 developer, Remover 1165, and Omnicoat adhesion promoter were purchased from KayukaAM. FcMeOH (97%) was purchased from Sigma-Aldrich, tetrabutylammonium hexafluorophosphate (98%) was purchased from TCI Chemicals, and potassium nitrate (reagent grade) was purchased from VWR Life Sciences.

Software

The software component controls the fluidic and electrochemical modules through an API written in Python. We use an open-source Python library known as Hardpotato to control commercial potentiostats.[31] We also developed an additional Python API that controls the fluidic module of the Electrolab.[52] Arduino microcontrollers enable communication of the fluidic module with Python via serial communication. Instructions for installing and using the software module for the Electrolab are provided in Note S2. All Python and Arduino scripts used in this work are provided in Data S2.

Construction of the solution-handling robot

The fluidic module is built around an XYZ gantry robot that moves a custom assembly of three 3D-printed nozzles that are connected to fluidic components such as peristaltic pumps, pneumatic pumps, and solenoid valves. Fluidic hardware was controlled by a printed circuit board (PCB) that uses an Arduino Mega microcontroller to communicate with the computer via serial. The XYZ gantry robot was adapted from a commercial 3D printer frame. Several components of the fluidic module, including the PCB, peristaltic pumps, and reagent bottles, were mounted on laser-cut acrylic plates. An openable drag chain allowed wires and tubing to move with the gantry head while avoiding entanglement. Additional information about the design, installation, and individual components of the fluid module is provided in Note S3. PDF files for laser cut components and STL files for 3D-printed components are included in Data S1 and listed in Table S1.

Electrode fabrication and electrochemical measurements

Electrodes were fabricated on 4-in glass wafers (University Wafer) as described previously described.[33] Wafers were cleaned by first degreasing using acetone and isopropanol, followed by an RCA-1 cleaning. A metal layer defining the electrode connections and wiring was patterned through

photolithography of an SPR-220 and LOR5A bilayer resist stack, followed by subsequent sputtering of platinum and liftoff in Remover 1165. Following liftoff, the surface was again RCA-1 cleaned before depositing an insulating SiO_2 layer via plasma-enhanced chemical vapor deposition (PECVD). KMPR 1010 epoxy resin was patterned photolithographically to define the electrode connections and electroactive regions. PECVD oxide underlayers were etched through using CF_4 plasma. Following patterning, the wafers were spin coated with a protective layer of SPR-220 photoresist and diced into individual devices using a dicing saw. The protective resist was removed from diced devices by degreasing. Connections to flexible ribbon cables were made using anisotropic conductive film (3M). Electrochemical cells were 3D printed using a resin 3D printer, and microfabricated electrodes were mounted in the cells, with an elastomer O-ring providing a leak-proof seal. Optical and atomic force micrographs of a microfabricated electrode are shown in Figures S2 and S3, respectively. A gold UME was fabricated by heat sealing 25-μm gold wire (99.99%, Goodfellow) in a glass capillary (World Precision Instruments), followed by sanding and polishing with progressively finer abrasives, from silicon carbide paper down to a 0.05-μm alumina slurry.

A CH Instruments model 760E bipotentiostat was used for all electrochemical experiments. Microfabricated electrodes were plasma cleaned in oxygen plasma for 5 min to remove organics prior to use and cycled in 0.1 M phosphate buffer solution at pH 7.4 to reduce any platinum oxide on the electrode surface. Electrochemical measurements with microfabricated devices used integrated platinum quasi-reference and counter electrodes on the chip. Measurements made with the gold UME were performed in a two-electrode configuration, using a platinum wire as a quasi-reference counter electrode. TE 100 screen-printed electrodes from CH instruments had carbon paste working and counter electrodes and a silver paste reference electrode. STL files of the electrochemical cells and a GDSII file of the microfabricated electrode design are included in Data S1.

SUPPLEMENTAL INFORMATION

Supplemental information can be found online at https://doi.org/10.1016/j.device.2023.100103.

ACKNOWLEDGMENTS

The research was financially supported by the Joint Center for Energy Storage Research (JCESR), an Energy Innovation Hub funded by the U.S. Department of Energy, Office of Science, Basic Energy Sciences. The material presented in this work was carried out in part in the Micro-Nano-Mechanical Systems Cleanroom Laboratory and the Holoynak Micro-Nano Technology Laboratory at the University of Illinois. We graciously thank A.I.B. Romo for providing the FeRAP, H. Nguyen for thoughtful discussions, and B. Ocampo for assistance with code.

AUTHOR CONTRIBUTIONS

All authors discussed the results and commented on the manuscript. I.O., M.A.P., N.G.L., and O.R. were responsible for methodology development and investigation. I.O., N.G.L., and O.R. were responsible for the development of software presented in this work. I.O. and M.A.P. were responsible for validation, formal analysis, visualization, and writing of the original manuscript draft. C.M.S. and J.R.-L. were responsible for conceptualization, funding acquisition, project administration, supervision, provision of resources, and review and editing of the manuscript.

DECLARATION OF INTERESTS

The authors declare no competing interests.

INCLUSION AND DIVERSITY

We support inclusive, diverse, and equitable conduct of research.

Received: July 28, 2023
Revised: August 27, 2023
Accepted: September 18, 2023
Published: October 10, 2023

REFERENCES

1. Crabtree, G. (2020). Self-Driving Laboratories Coming of Age. Joule *4*, 2538–2541. https://doi.org/10.1016/j.joule.2020.11.021.
2. Li, S., Jira, E.R., Angello, N.H., Li, J., Yu, H., Moore, J.S., Diao, Y., Burke, M.D., and Schroeder, C.M. (2022). Using automated synthesis to understand the role of side chains on molecular charge transport. Nat. Commun. *13*, 2102. https://doi.org/10.1038/s41467-022-29796-2.
3. Jiang, Y., Salley, D., Sharma, A., Keenan, G., Mullin, M., and Cronin, L. (2022). An artificial intelligence enabled chemical synthesis robot for exploration and optimization of nanomaterials. Sci. Adv. *8*, eabo2626. https://doi.org/10.1126/sciadv.abo2626.
4. MacLeod, B.P., Parlane, F.G.L., Morrissey, T.D., Häse, F., Roch, L.M., Dettelbach, K.E., Moreira, R., Yunker, L.P.E., Rooney, M.B., Deeth, J.R., et al. (2020). Self-driving laboratory for accelerated discovery of thin-film materials. Sci. Adv. *6*, eaaz8867. https://doi.org/10.1126/sciadv.aaz8867.
5. Li, M., Case, J., and Minteer, S.D. (2021). Bipolar Redox-Active Molecules in Non-Aqueous Organic Redox Flow Batteries: Status and Challenges. Chemelectrochem *8*, 1215–1232. https://doi.org/10.1002/celc.202001584.
6. Winsberg, J., Hagemann, T., Janoschka, T., Hager, M.D., and Schubert, U.S. (2017). Redox-Flow Batteries: From Metals to Organic Redox-Active Materials. Angew. Chem. Int. Ed. *56*, 686–711. https://doi.org/10.1002/anie.201604925.
7. Kowalski, J.A., Su, L., Milshtein, J.D., and Brushett, F.R. (2016). Recent advances in molecular engineering of redox active organic molecules for nonaqueous flow batteries. Curr. Opin. Chem. Eng. *13*, 45–52. https://doi.org/10.1016/j.coche.2016.08.002.
8. Er, S., Suh, C., Marshak, M.P., and Aspuru-Guzik, A. (2015). Computational design of molecules for an all-quinone redox flow battery. Chem. Sci. *6*, 885–893. https://doi.org/10.1039/C4SC03030C.
9. Burgess, M., Moore, J.S., and Rodríguez-López, J. (2016). Redox Active Polymers as Soluble Nanomaterials for Energy Storage. Acc. Chem. Res. *49*, 2649–2657. https://doi.org/10.1021/acs.accounts.6b00341.
10. Hendriks, K.H., Robinson, S.G., Braten, M.N., Sevov, C.S., Helms, B.A., Sigman, M.S., Minteer, S.D., and Sanford, M.S. (2018). High-Performance Oligomeric Catholytes for Effective Macromolecular Separation in Nonaqueous Redox Flow Batteries. ACS Cent. Sci. *4*, 189–196. https://doi.org/10.1021/acscentsci.7b00544.
11. Montoto, E.C., Nagarjuna, G., Hui, J., Burgess, M., Sekerak, N.M., Hernández-Burgos, K., Wei, T.-S., Kneer, M., Grolman, J., Cheng, K.J., et al. (2016). Redox Active Colloids as Discrete Energy Storage Carriers. J. Am. Chem. Soc. *138*, 13230–13237. https://doi.org/10.1021/jacs.6b06365.
12. Yan, Y., Zhang, L., Walser-Kuntz, R., Vogt, D.B., Sigman, M.S., Yu, G., and Sanford, M.S. (2022). Benzotriazoles as Low-Potential Anolytes for Nonaqueous Redox Flow Batteries. Chem. Mater. *34*, 10594–10605. https://doi.org/10.1021/acs.chemmater.2c02682.
13. Robinson, S.G., Yan, Y., Hendriks, K.H., Sanford, M.S., and Sigman, M.S. (2019). Developing a Predictive Solubility Model for Monomeric and Oligomeric Cyclopropenium-Based Flow Battery Catholytes. J. Am. Chem. Soc. *141*, 10171–10176. https://doi.org/10.1021/jacs.9b04270.
14. Hatakeyama-Sato, K., Igarashi, Y., and Oyaizu, K. (2022). Charge-transport kinetics of dissolved redox-active polymers for rational design of flow batteries. RSC Adv. *13*, 547–557. https://doi.org/10.1039/D2RA07208D.
15. Cheng, L., Assary, R.S., Qu, X., Jain, A., Ong, S.P., Rajput, N.N., Persson, K., and Curtiss, L.A. (2015). Accelerating Electrolyte Discovery for Energy

Storage with High-Throughput Screening. J. Phys. Chem. Lett. *6*, 283–291. https://doi.org/10.1021/jz502319n.

16. Huang, J., Pan, B., Duan, W., Wei, X., Assary, R.S., Su, L., Brushett, F.R., Cheng, L., Liao, C., Ferrandon, M.S., et al. (2016). The lightest organic radical cation for charge storage in redox flow batteries. Sci. Rep. *6*, 32102. https://doi.org/10.1038/srep32102.
17. Goulet, M.-A., Tong, L., Pollack, D.A., Tabor, D.P., Odom, S.A., Aspuru-Guzik, A., Kwan, E.E., Gordon, R.G., and Aziz, M.J. (2019). Extending the Lifetime of Organic Flow Batteries via Redox State Management. J. Am. Chem. Soc. *141*, 8014–8019. https://doi.org/10.1021/jacs.8b13295.
18. Burgess, M., Hernández-Burgos, K., Schuh, J.K., Davila, J., Montoto, E.C., Ewoldt, R.H., and Rodríguez-López, J. (2018). Modulation of the Electrochemical Reactivity of Solubilized Redox Active Polymers via Polyelectrolyte Dynamics. J. Am. Chem. Soc. *140*, 2093–2104. https://doi.org/10.1021/jacs.7b08353.
19. Zhao, E.W., Jónsson, E., Jethwa, R.B., Hey, D., Lyu, D., Brookfield, A., Klusener, P.A.A., Collison, D., and Grey, C.P. (2021). Coupled In Situ NMR and EPR Studies Reveal the Electron Transfer Rate and Electrolyte Decomposition in Redox Flow Batteries. J. Am. Chem. Soc. *143*, 1885–1895. https://doi.org/10.1021/jacs.0c10650.
20. Fell, E., and Aziz, M. (2023). High-Throughput Electrochemical Characterization of Aqueous Organic Redox Flow Battery Active Material. Preprint at ChemRxiv. https://doi.org/10.26434/chemrxiv-2023-3vbn6.
21. Jia, S., Counsell, J., Adamič, M., Jonderian, A., and McCalla, E. (2022). High-throughput design of Na–Fe–Mn–O cathodes for Na-ion batteries. J. Mater. Chem. A *10*, 251–265. https://doi.org/10.1039/D1TA07940A.
22. Dave, A., Mitchell, J., Burke, S., Lin, H., Whitacre, J., and Viswanathan, V. (2022). Autonomous optimization of nonaqueous battery electrolytes via robotic experimentation and machine learning. Nat. Commun. *13*, 5454. https://doi.org/10.1038/s41467-022-32938-1.
23. Su, L., Ferrandon, M., Kowalski, J.A., Vaughey, J.T., and Brushett, F.R. (2014). Electrolyte Development for Non-Aqueous Redox Flow Batteries Using a High-Throughput Screening Platform. J. Electrochem. Soc. *161*, A1905–A1914. https://doi.org/10.1149/2.0811412jes.
24. Duke, R., Mahmoudi, S., Kaur, A.P., Bhat, V., Dingle, I., Stumme, N., Shaw, S., Eaton, D., Vego, A., and Risko, C. (2023). Towards Reproducible and Automated Electrochemistry. Preprint at ChemRxiv. https://doi.org/10.26434/chemrxiv-2023-cds00.
25. Ryabova, V., Schulte, A., Erichsen, T., and Schuhmann, W. (2005). Robotic sequential analysis of a library of metalloporphyrins as electrocatalysts for voltammetric nitric oxide sensors. Analyst *130*, 1245–1252. https://doi.org/10.1039/B505284J.
26. Erichsen, T., Reiter, S., Ryabova, V., Bonsen, E.M., Schuhmann, W., Märkle, W., Tittel, C., Jung, G., and Speiser, B. (2005). Combinatorial microelectrochemistry: Development and evaluation of an electrochemical robotic system. Rev. Sci. Instrum. *76*, 062204. https://doi.org/10.1063/1.1906106.
27. Lindner, E., Lu, Z.-L., Mayer, H.A., Speiser, B., Tittel, C., and Warad, I. (2005). Combinatorial micro electrochemistry. Part 4: Cyclic voltammetric redox screening of homogeneous ruthenium(II) hydrogenation catalysts. Electrochem. Commun. *7*, 1013–1020. https://doi.org/10.1016/j.elecom.2005.07.002.
28. Godfrey, D., Bannock, J.H., Kuzmina, O., Welton, T., and Albrecht, T. (2016). A robotic platform for high-throughput electrochemical analysis of chalcopyrite leaching. Green Chem. *18*, 1930–1937. https://doi.org/10.1039/C5GC02306H.
29. Gerroll, B.H.R., Kulesa, K.M., Ault, C.A., and Baker, L.A. (2023). Legion: An Instrument for High-Throughput Electrochemistry. ACS Meas. Sci. Au. https://doi.org/10.1021/acsmeasuresciau.3c00022.
30. Wightman, R.M. (1988). Voltammetry with Microscopic Electrodes in New Domains. Science *240*, 415–420. https://doi.org/10.1126/science.240.4851.415.
31. Rodríguez, O., Pence, M.A., and Rodríguez-López, J. (2023). Hard Potato: A Python Library to Control Commercial Potentiostats and to Automate Electrochemical Experiments. Anal. Chem. *95*, 4840–4845. https://doi.org/10.1021/acs.analchem.2c04862.
32. Watkins, T.S., Sarbapalli, D., Counihan, M.J., Danis, A.S., Zhang, J., Zhang, L., Zavadil, K.R., and Rodríguez-López, J. (2020). A combined SECM and electrochemical AFM approach to probe interfacial processes affecting molecular reactivity at redox flow battery electrodes. J. Mater. Chem. A *8*, 15734–15745. https://doi.org/10.1039/D0TA00836B.
33. Pence, M.A., Rodríguez, O., Lukhanin, N.G., Schroeder, C.M., and Rodríguez-López, J. (2023). Automated Measurement of Electrogenerated Redox Species Degradation Using Multiplexed Interdigitated Electrode Arrays. ACS Meas. Sci. Au *3*, 62–72. https://doi.org/10.1021/acsmeasuresciau.2c00054.
34. Cannes, C., Kanoufi, F., and Bard, A.J. (2003). Cyclic voltammetry and scanning electrochemical microscopy of ferrocenemethanol at monolayer and bilayer-modified gold electrodes. J. Electroanal. Chem. *547*, 83–91. https://doi.org/10.1016/S0022-0728(03)00192-X.
35. Chen, L., Kätelhön, E., and Compton, R.G. (2019). Unscrambling illusory inhibition and catalysis in nanoparticle electrochemistry: Experiment and theory. Appl. Mater. Today *16*, 141–145. https://doi.org/10.1016/j.apmt.2019.05.002.
36. Miao, W., Ding, Z., and Bard, A.J. (2002). Solution Viscosity Effects on the Heterogeneous Electron Transfer Kinetics of Ferrocenemethanol in Dimethyl Sulfoxide−Water Mixtures. J. Phys. Chem. B *106*, 1392–1398. https://doi.org/10.1021/jp013451u.
37. Amatore, C., Da Mota, N., Sella, C., and Thouin, L. (2007). Theory and Experiments of Transport at Channel Microband Electrodes under Laminar Flows. 1. Steady-State Regimes at a Single Electrode. Anal. Chem. *79*, 8502–8510. https://doi.org/10.1021/ac070971y.
38. Sun, P., and Mirkin, M.V. (2006). Kinetics of Electron-Transfer Reactions at Nanoelectrodes. Anal. Chem. *78*, 6526–6534. https://doi.org/10.1021/ac060924q.
39. Nicholson, R.S., and Shain, I. (1964). Theory of Stationary Electrode Polarography. Single Scan and Cyclic Methods Applied to Reversible, Irreversible, and Kinetic Systems. Anal. Chem. *36*, 706–723. https://doi.org/10.1021/ac60210a007.
40. Bard, A.J., Faulkner, L.R., and White, H.S. (2022). Electrochemical Methods: Fundamentals and Applications, 3rd ed. (John Wiley & Sons, Ltd).
41. Burgess, M., Hernández-Burgos, K., Simpson, B.H., Lichtenstein, T., Avetian, S., Nagarjuna, G., Cheng, K.J., Moore, J.S., and Rodríguez-López, J. (2015). Scanning Electrochemical Microscopy and Hydrodynamic Voltammetry Investigation of Charge Transfer Mechanisms on Redox Active Polymers. J. Electrochem. Soc. *163*, H3006–H3013. https://doi.org/10.1149/2.0021604jes.
42. Bello, L., and Sing, C.E. (2020). Mechanisms of Diffusive Charge Transport in Redox-Active Polymer Solutions. Macromolecules *53*, 7658–7671. https://doi.org/10.1021/acs.macromol.0c01672.
43. Chen, H., Kätelhön, E., and Compton, R.G. (2023). Machine learning in fundamental electrochemistry: Recent advances and future opportunities. Curr. Opin. Electrochem. *38*, 101214. https://doi.org/10.1016/j.coelec.2023.101214.
44. Kennedy, G.F., Zhang, J., and Bond, A.M. (2019). Automatically Identifying Electrode Reaction Mechanisms Using Deep Neural Networks. Anal. Chem. *91*, 12220–12227. https://doi.org/10.1021/acs.analchem.9b01891.
45. Hoar, B.B., Zhang, W., Xu, S., Deeba, R., Costentin, C., Gu, Q., and Liu, C. (2022). Electrochemical Mechanistic Analysis from Cyclic Voltammograms Based on Deep Learning. ACS Meas. Sci. Au *2*, 595–604. https://doi.org/10.1021/acsmeasuresciau.2c00045.
46. Angello, N.H., Rathore, V., Beker, W., Wołos, A., Jira, E.R., Roszak, R., Wu, T.C., Schroeder, C.M., Aspuru-Guzik, A., Grzybowski, B.A., and

Burke, M.D. (2022). Closed-loop optimization of general reaction conditions for heteroaryl Suzuki-Miyaura coupling. Science *378*, 399–405. https://doi.org/10.1126/science.adc8743.

47. Shields, B.J., Stevens, J., Li, J., Parasram, M., Damani, F., Alvarado, J.I.M., Janey, J.M., Adams, R.P., and Doyle, A.G. (2021). Bayesian reaction optimization as a tool for chemical synthesis. Nature *590*, 89–96. https://doi.org/10.1038/s41586-021-03213-y.

48. Baker, M. (2016). 1,500 scientists lift the lid on reproducibility. Nature *533*, 452–454. https://doi.org/10.1038/533452a.

49. Smith, G., and Dickinson, E.J.F. (2022). Error, reproducibility and uncertainty in experiments for electrochemical energy technologies. Nat. Commun. *13*, 6832. https://doi.org/10.1038/s41467-022-34594-x.

50. Hammer, A.J.S., Leonov, A.I., Bell, N.L., and Cronin, L. (2021). Chemputation and the Standardization of Chemical Informatics. JACS Au *1*, 1572–1587. https://doi.org/10.1021/jacsau.1c00303.

51. Oh, I., Pence, M., Lukhanin, N., Rodríguez, O., Schroeder, C., and Rodríguez-López, J. (2023). Data from 'The Electrolab: An open-source, modular platform for automated characterization of redox-active electrolytes'. Preprint at Mendeley Data. https://doi.org/10.17632/cvm9y582tf.1.

52. Oh, I., Pence, M., Lukhanin, N., Rodríguez, O., Schroeder, C., and Rodríguez-López, J. (2023). jrlLAB/ElectroLab: API to control the ElectroLab. Preprint at Zenodo. https://doi.org/10.5281/zenodo.8323222.